Supporting Information

Fluorinated *B*-phenylated scorpionates as tunable platforms for stabilizing thallium(I) and silver(I)-ethylene complexes

Anurag Noonikara-Poyil,[a] Vo Quang Huy Phan,[a] Mukundam Vanga,[a] Andrii Boretskyi,[b] Pavel Mykhailiuk,[b,c*] H. V. Rasika Dias[a,*]

[a] Department of Chemistry and Biochemistry, The University of Texas at Arlington, Arlington, Texas 76019, USA;

Email: dias@uta.edu

[b] Enamine Ltd., Winston Churchill St. 78, 02094, Kyiv, Ukraine.

[c] Chemistry Department, Taras Shevchenko National University of Kyiv Volodymyrska 64, 01601 Kyiv, Ukraine;

E-mail: Pavel.Mykhailiuk@gmail.com

Table of contents:

Table S1. Selected structural and spectroscopic parameters of thallium complexes supported by fluorinated tris- and bis(pyrazolyl/pyridyl)borate, with -CF_3 and -SF_5 groups around thallium. Fc = ferrocenyl.

Compound	δ (ppm) *(solvent)*	multiplicity	J_{Tl-F} (Hz)	Tl•••CF_3 (avg.) (Å)	Ref.
[$Ph_2B(3\text{-}(CF_3)Pz)_2$]Tl (4)	**-60.2** *($CDCl_3$)*	**d**	**576**	**3.997**	[1] **This work**
[$Ph_2B(3\text{-}(SF_5)Pz)_2$]Tl (5)	**82.8, 65.5** *($CDCl_3$)*	**pd dd**	**76, 777**	**N/A**	[1]
[$H_2B(3,5\text{-}(CF_3)_2Pz)_2$]Tl	-61.1, -58.9 *(CD_3CN)*	s s	N/A	4.213	[2, 3]
[$PhB(3\text{-}(CF_3)Pz)_3$]Tl	-60.7 *($CDCl_3$)*	br d	388	4.07	[4]
[$HB(3\text{-}(CF_3),5\text{-}(Fc)Pz)_3$]Tl	-59.2 *(N/A)*	d	821	3.832	[5]
[$HB(3\text{-}(CF_3),5\text{-}(thienyl)Pz)_3$]Tl	-60.6 *($CDCl_3$)*	d	850	3.796	[6]
[$HB(3,5\text{-}(CF_3)_2Pz)_3$]Tl	-60.0 *($CDCl_3$)*	br d	870	3.775	[3]
[$MeB(3\text{-}(CF_3)Pz)_3$]Tl	-59.1 *($CDCl_3$)*	d	878	3.786	[7]
[$HB(3\text{-}(CF_3),5\text{-}(Ph)Pz)_3$]Tl	-59.3 *($CDCl_3$)*	d	880	3.821	[8] This work
[$HB(4\text{-}Br\text{-}3,5\text{-}(CF_3)_2Pz)_3$]Tl	-60.0 *($CDCl_3$)*	d	972	3.894	[9]
[$Ph_2B(6\text{-}(CF_3)Py)_2$]Tl (6)	**-65.3** *($CDCl_3$)*	**d**	**1100**	**3.585**	**This work**
[$PhB(6\text{-}(CF_3)Py)_3$]Tl	-64.5 *($CDCl_3$)*	d	1110	3.57	[4]
[$MeB(6\text{-}(CF_3)Py)_3$]Tl	-64.5 *($CDCl_3$)*	d	1208	3.45	[4]

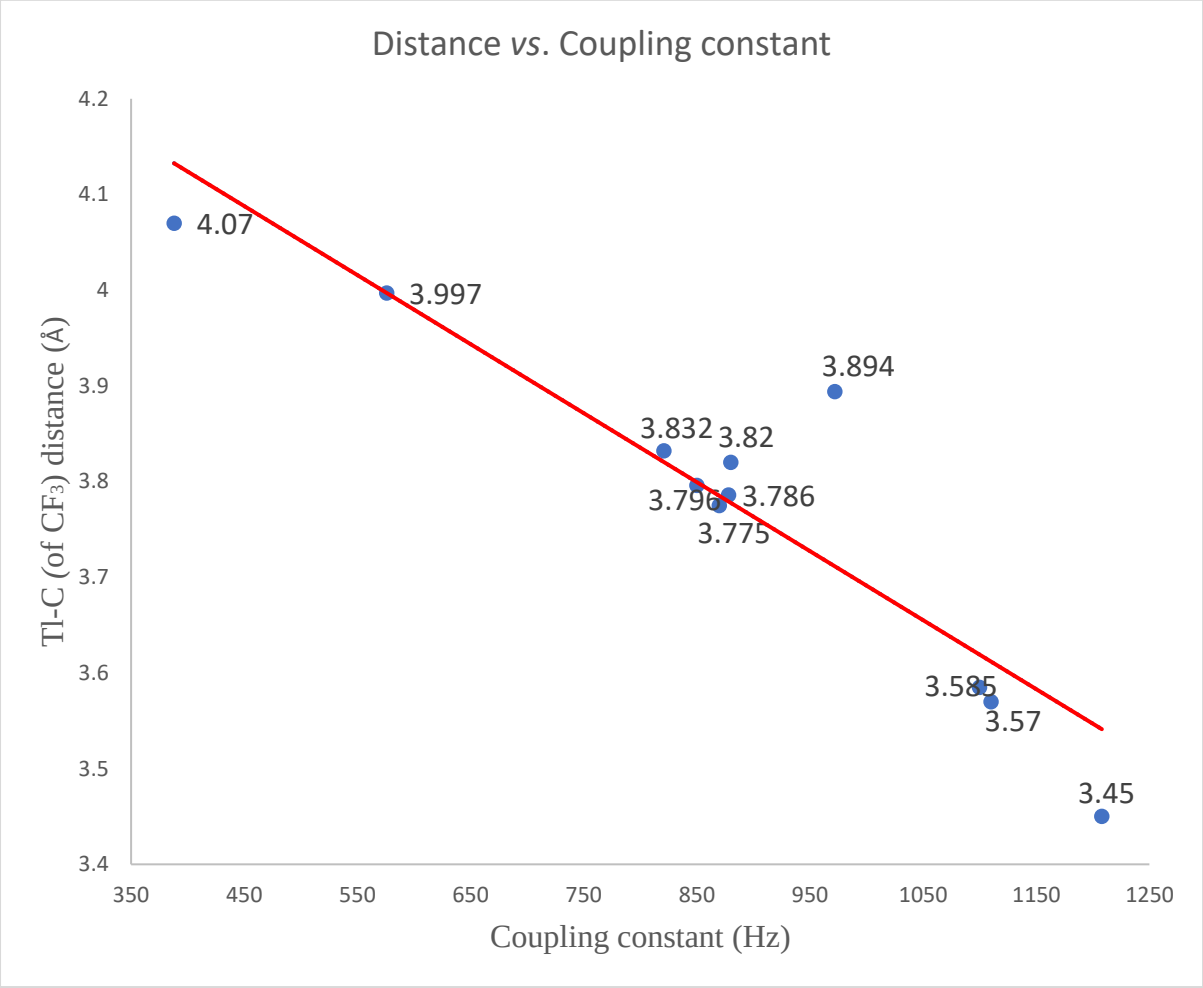

Figure S1. Plot showing the correlation between the $J_{Tl\text{-}F}$ coupling constant and the Tl•••CF_3 distance, generated from the data summarized in Table S1.

Analysis of the topographic steric map

Computed using SambVca 2.1[10] for a sphere radius of 3.5 Å about the metal center, Bondi van der Waals radii scaled by a factor of 1.17, 0.10 Å mesh spacing, and including hydrogen atoms (difference in $\%V_{Bur}$ value was negligible (≤0.1%) between inclusion or omission of H-atoms in these molecules during calculation). Per SambVca protocol, metal-ethylene moieties were removed for the calculation of steric maps and $\%V_{Bur}$

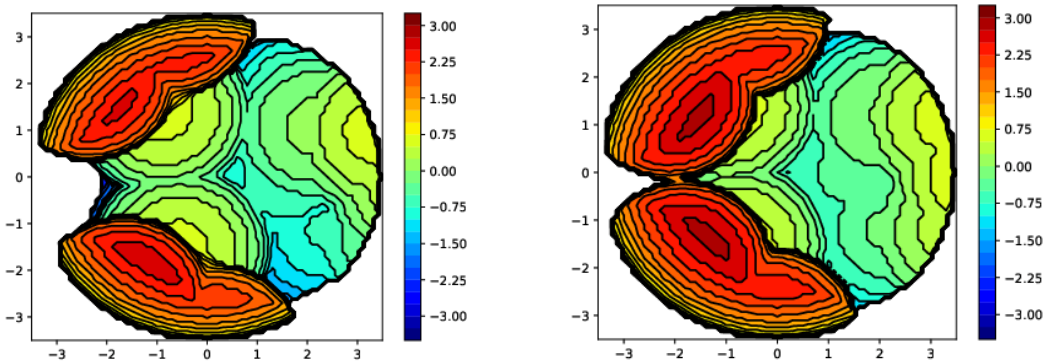

$[Ph_2B(3\text{-}(CF_3)Pz)_2]Cu(C_2H_4)$
($\%V_{Bur}$ = **59.5%)**

$[Ph_2B(3\text{-}(SF_5)Pz)_2]Cu(C_2H_4)$
($\%V_{Bur}$ = **65.6%)**

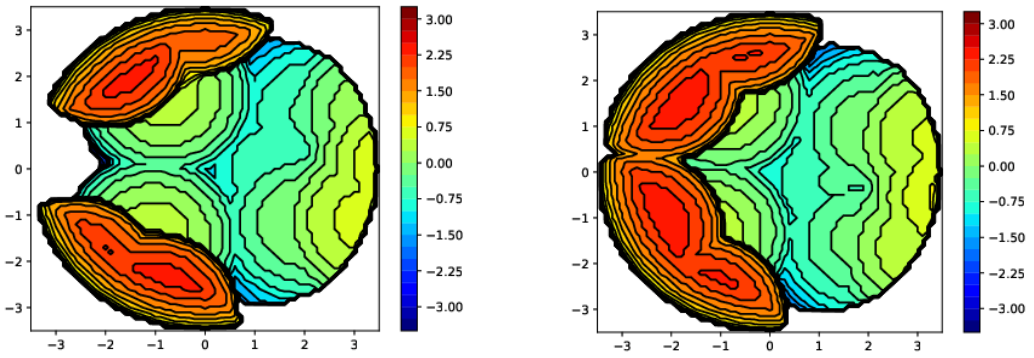

$[Ph_2B(3\text{-}(CF_3)Pz)_2]Ag(C_2H_4)$
($\%V_{Bur}$ = **55.0%)**

$[Ph_2B(3\text{-}(SF_5)Pz)_2]Ag(C_2H_4)$
($\%V_{Bur}$ = **61.4%)**

Figure S2. A comparison of the steric maps of supporting ligands in previously reported copper adducts $[Ph_2B(3\text{-}(CF_3)Pz)_2]Cu(C_2H_4)$ (top left),[1] and $[Ph_2B(3\text{-}(SF_5)Pz)_2]Cu(C_2H_4)$[1] (top right), to newly uncovered silver complexes $[Ph_2B(3\text{-}(CF_3)Pz)_2]Ag(C_2H_4)$ (**7**, bottom left), and $[Ph_2B(3\text{-}(SF_5)Pz)_2]Ag(C_2H_4)$ (**8**, bottom right). The resulting % buried volume values are 59.5%, 65.6%, 55.0%, and 61.4%, respectively.

NMR Spectroscopy

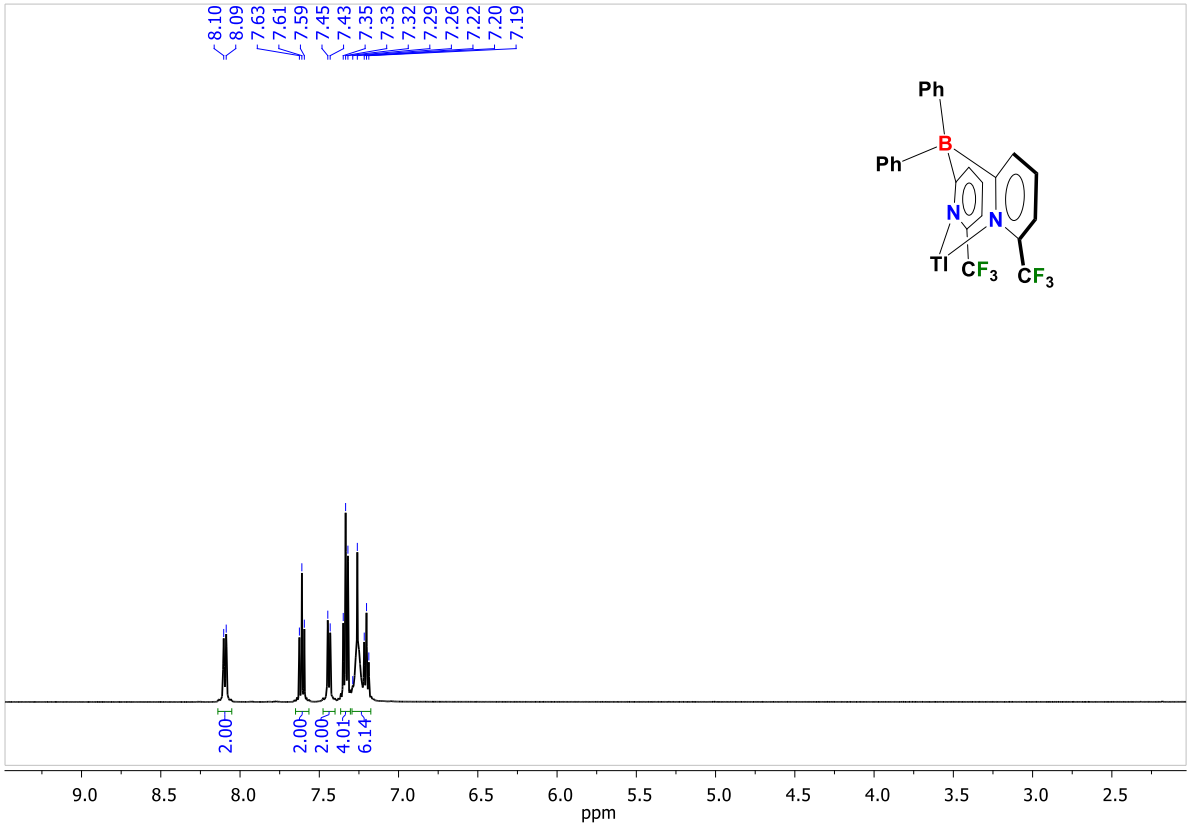

Figure S3. ^{1}H NMR spectrum of [$Ph_2B(6\text{-}(CF_3)Py)_2$]Tl (**6**) in $CDCl_3$

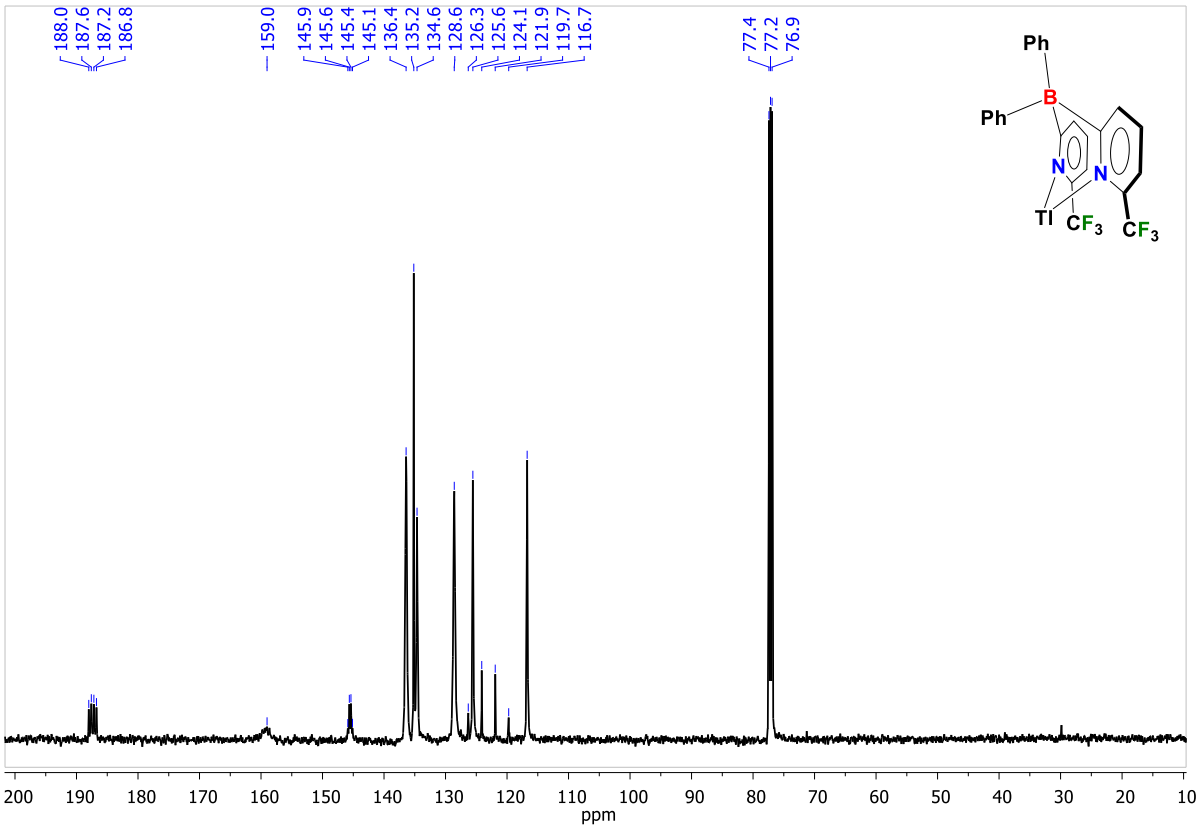

Figure S4. $^{13}C\{^{1}H\}$ NMR spectrum of $[Ph_2B(6\text{-}(CF_3)Py)_2]Tl$ (**6**) in $CDCl_3$

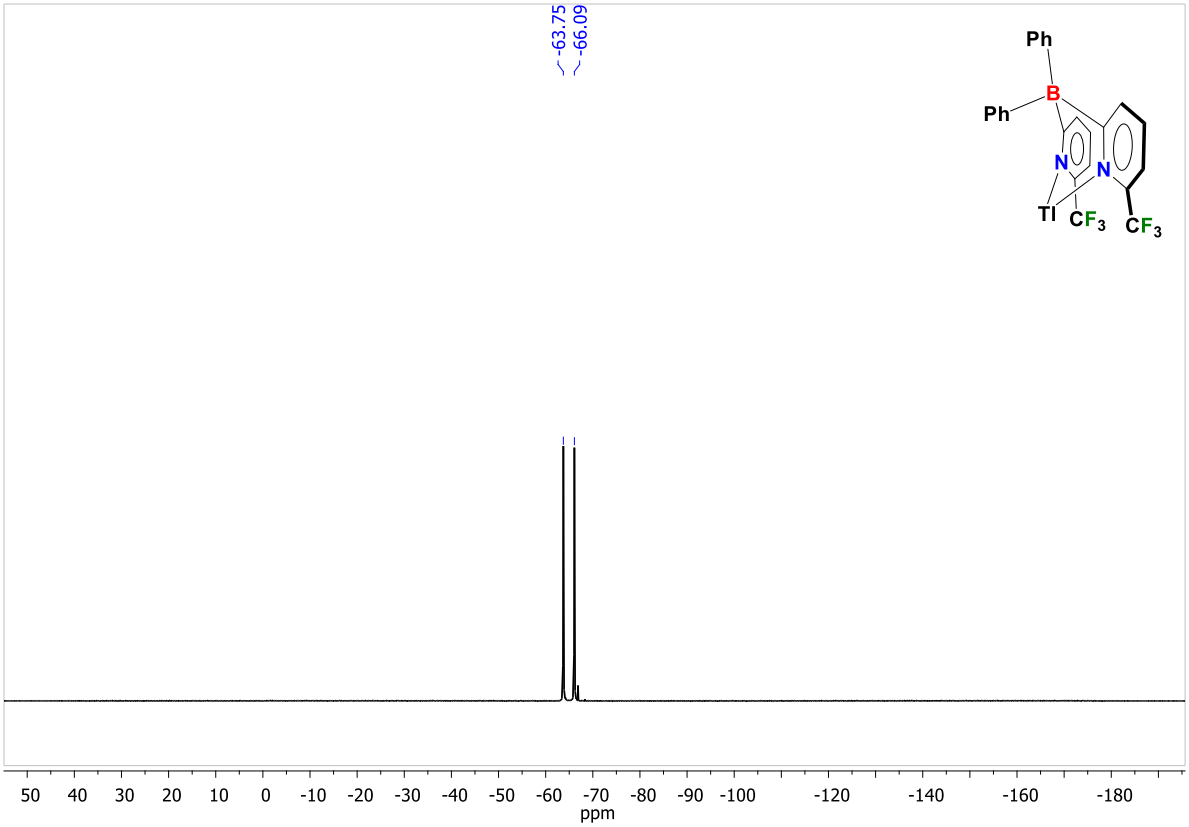

Figure S5. ^{19}F NMR spectrum of $[Ph_2B(6\text{-}(CF_3)Py)_2]Tl$ (**6**) in $CDCl_3$

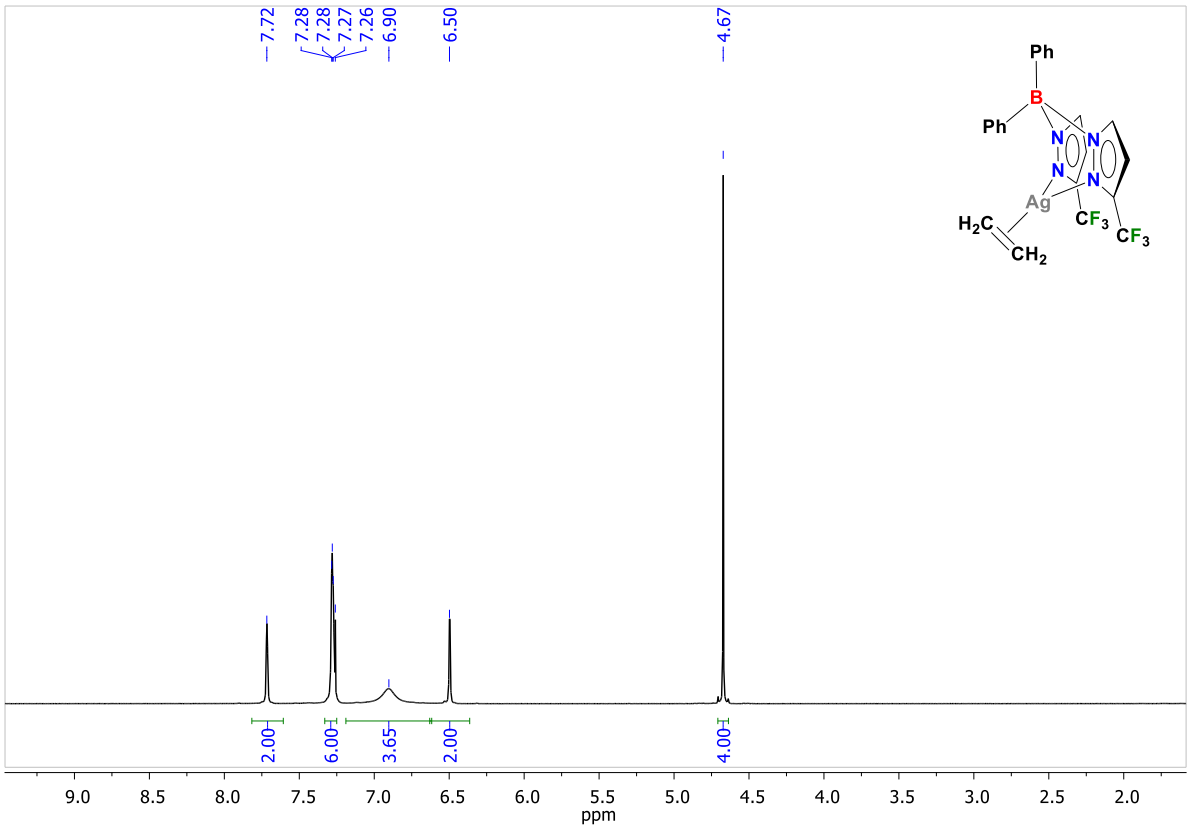

Figure S6. ^{1}H NMR Spectrum of $[Ph_2B(3\text{-}(CF_3)Pz)_2]Ag(C_2H_4)$ (**7**) in $CDCl_3$

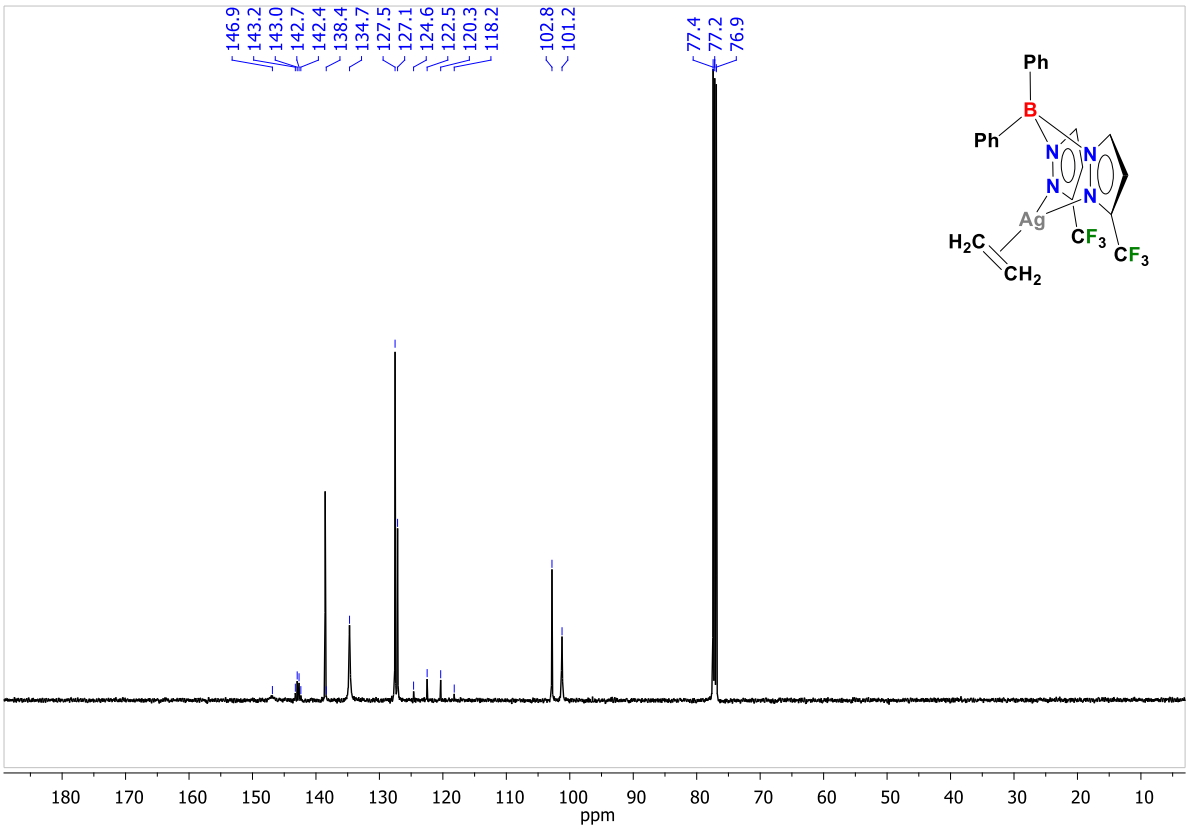

Figure S7. $^{13}C\{^{1}H\}$ NMR Spectrum of $[Ph_2B(3\text{-}(CF_3)Pz)_2]Ag(C_2H_4)$ (**7**) in $CDCl_3$

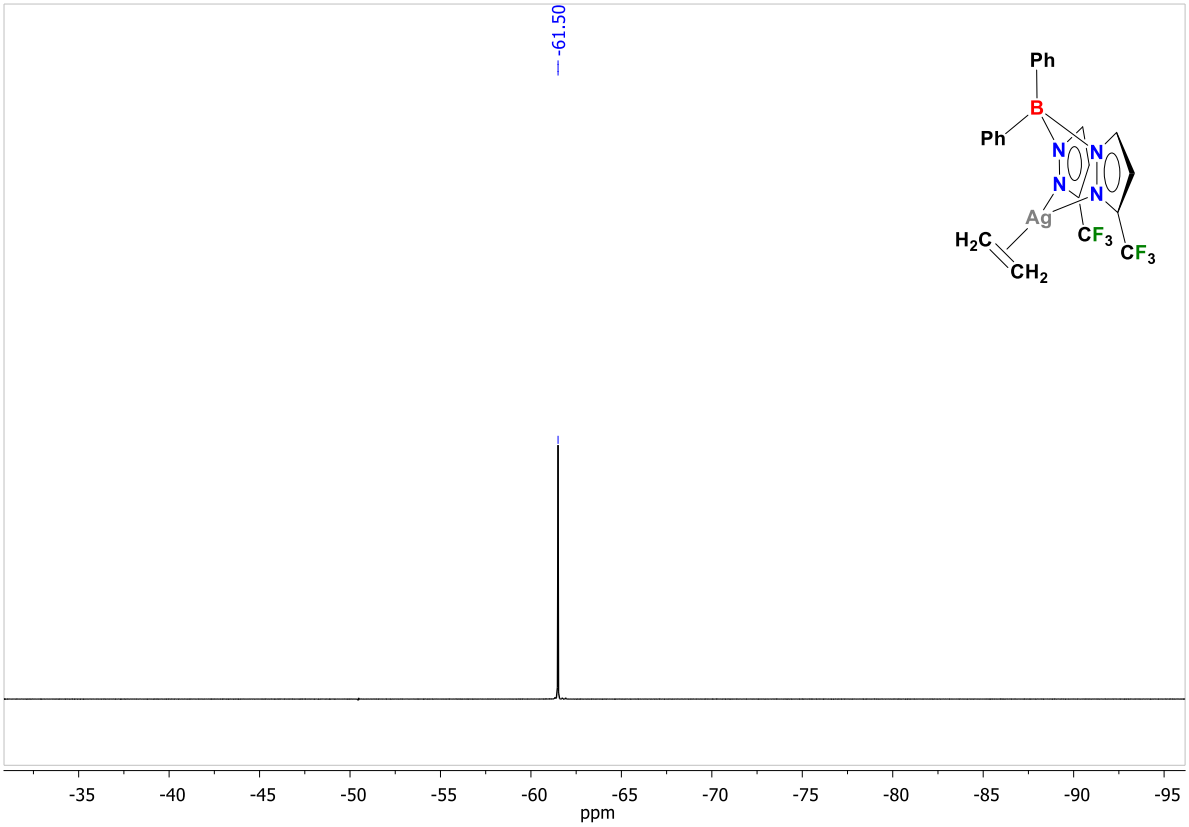

Figure S8. ^{19}F NMR Spectrum of $[Ph_2B(3\text{-}(CF_3)Pz)_2]Ag(C_2H_4)$ (**7**) in $CDCl_3$

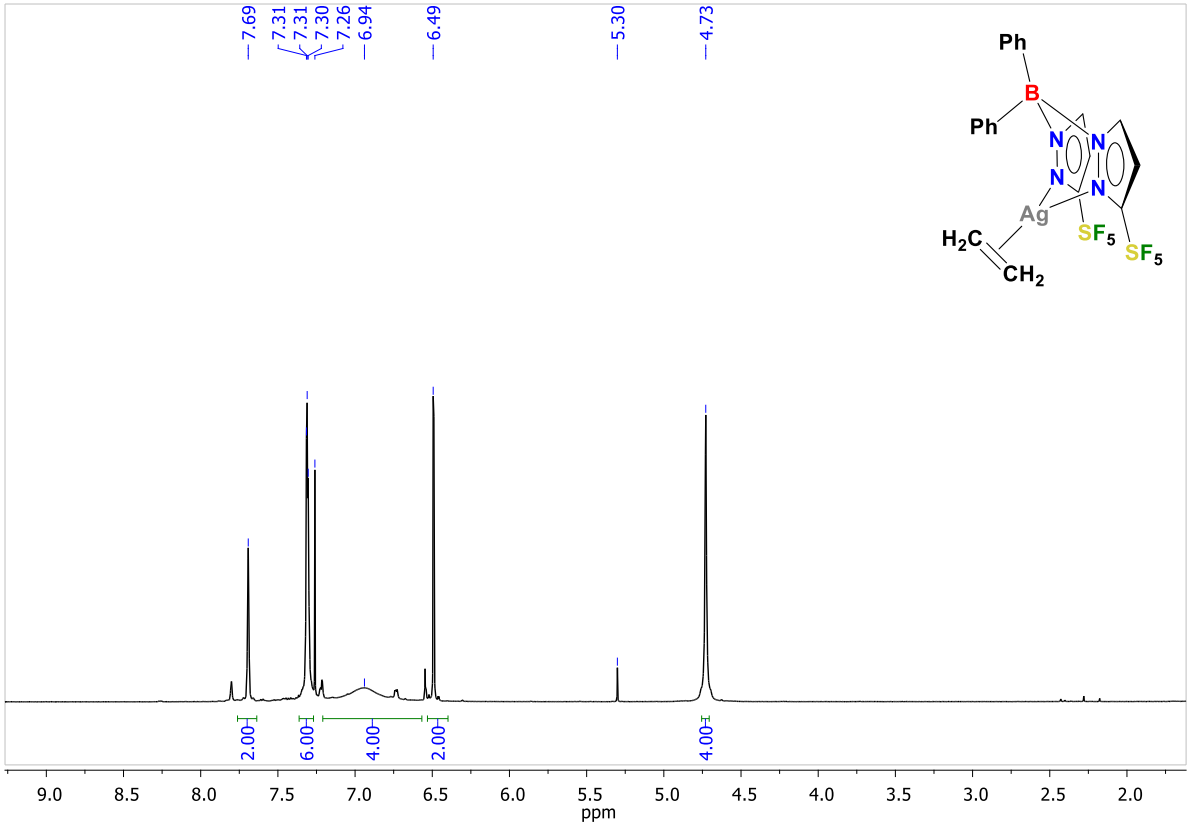

Figure S9. ^{1}H NMR Spectrum of $[Ph_2B(3\text{-}(SF_5)Pz)_2]Ag(C_2H_4)$ (**8**) in $CDCl_3$. Peak at 5.30 ppm belongs to trace DCM

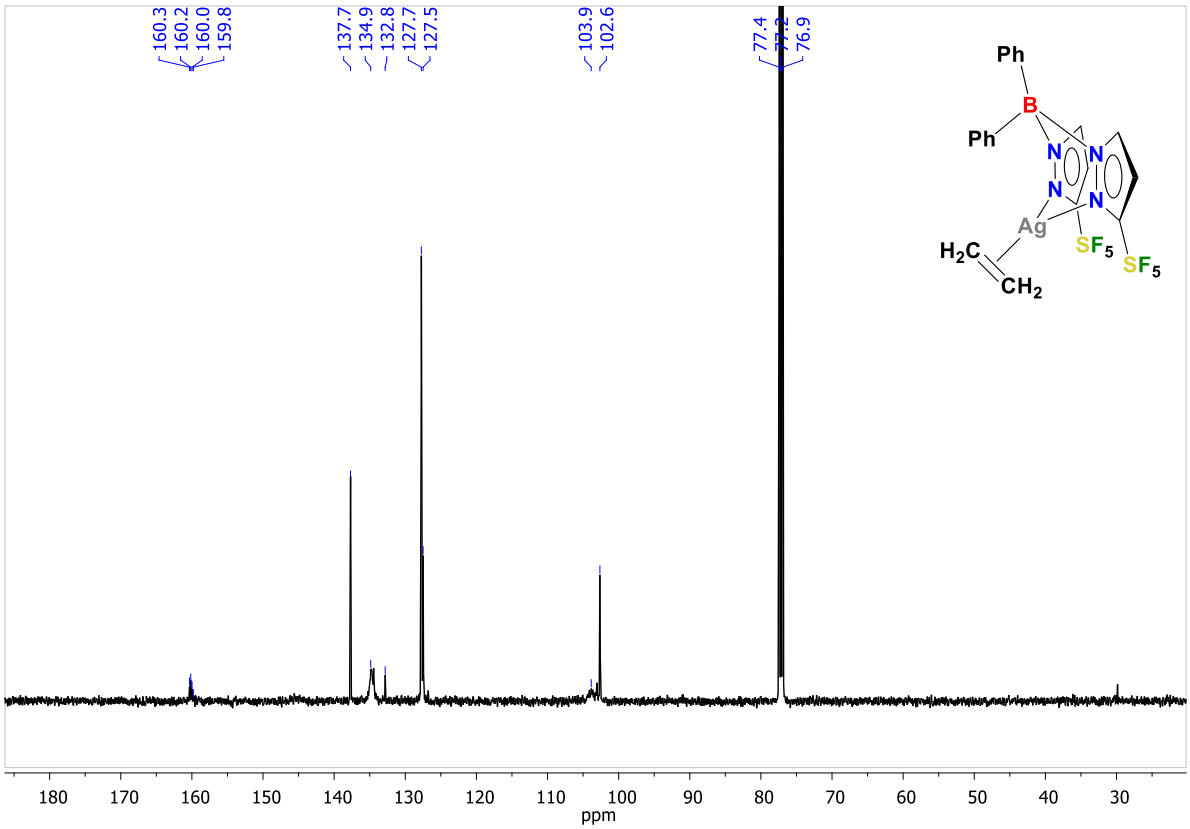

Figure S10. $^{13}C\{^{1}H\}$ NMR Spectrum of $[Ph_2B(3\text{-}(SF_5)Pz)_2]Ag(C_2H_4)$ (**8**) in $CDCl_3$

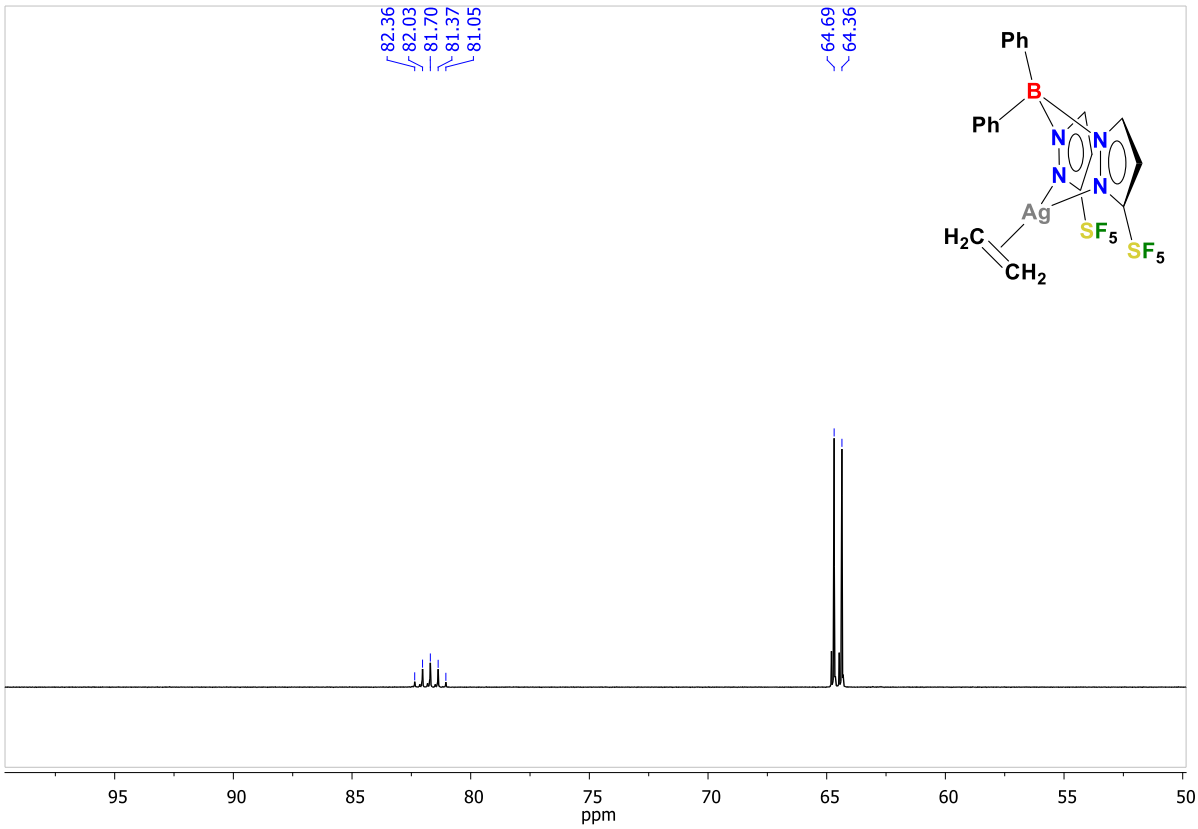

Figure S11. ^{19}F NMR Spectrum of $[Ph_2B(3\text{-}(SF_5)Pz)_2]Ag(C_2H_4)$ (**8**) in $CDCl_3$

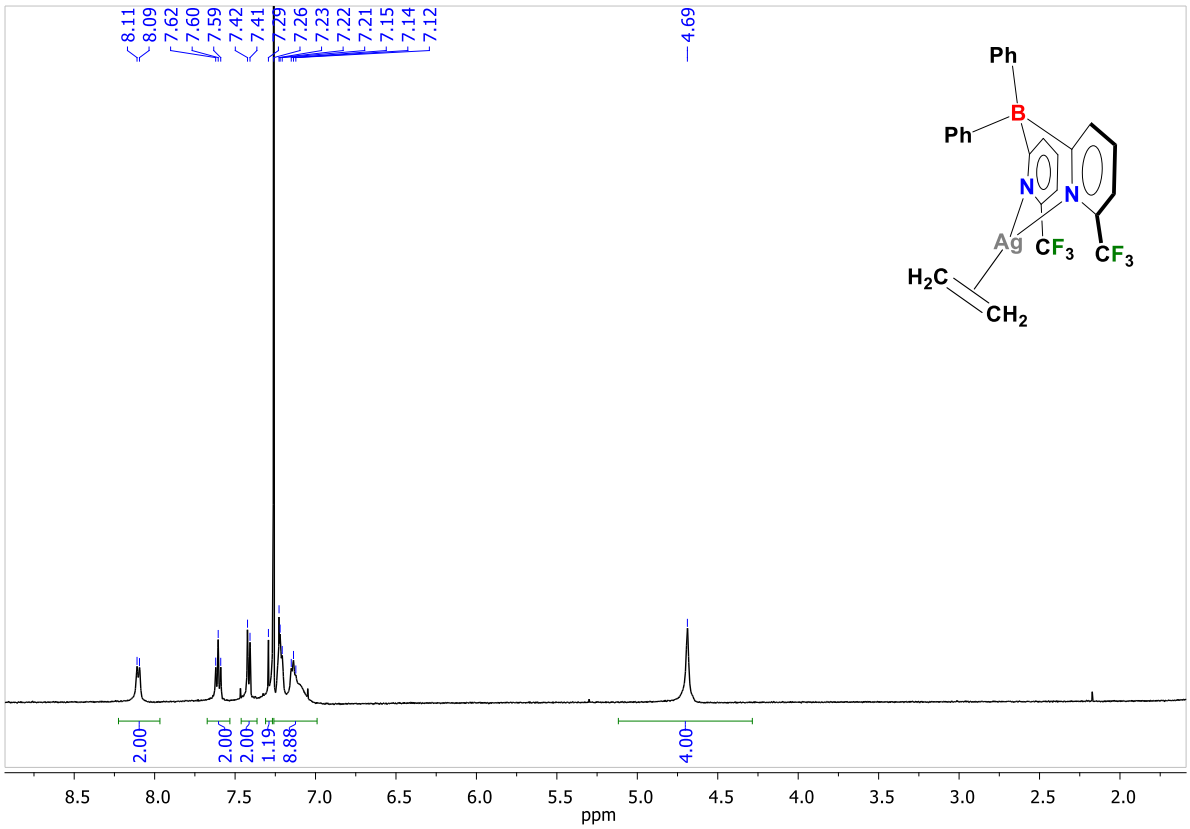

Figure S12. ^{1}H NMR spectrum of $[Ph_2B(6\text{-}(CF_3)Py)_2]Ag(C_2H_4)$ (**9**) in $CDCl_3$

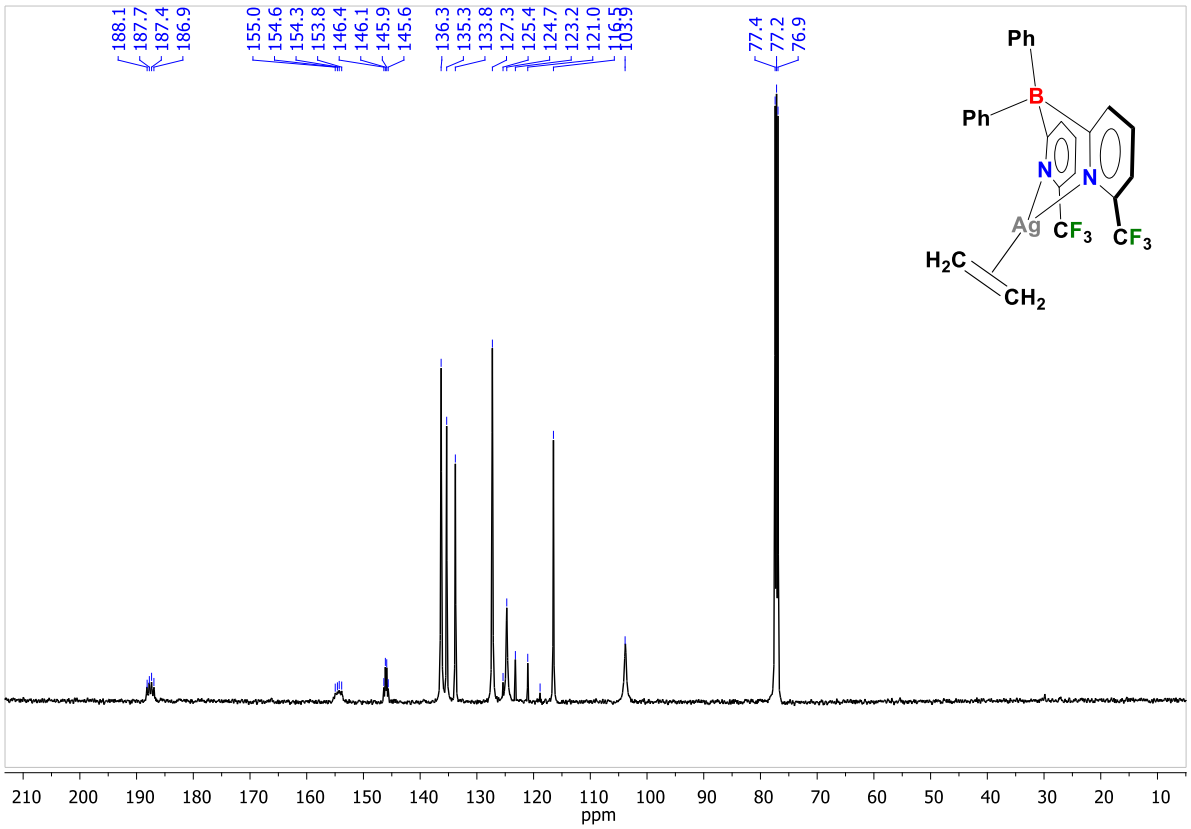

Figure S13. $^{13}C\{^{1}H\}$ NMR spectrum of $[Ph_2B(6\text{-}(CF_3)Py)_2]Ag(C_2H_4)$ (**9**) in $CDCl_3$

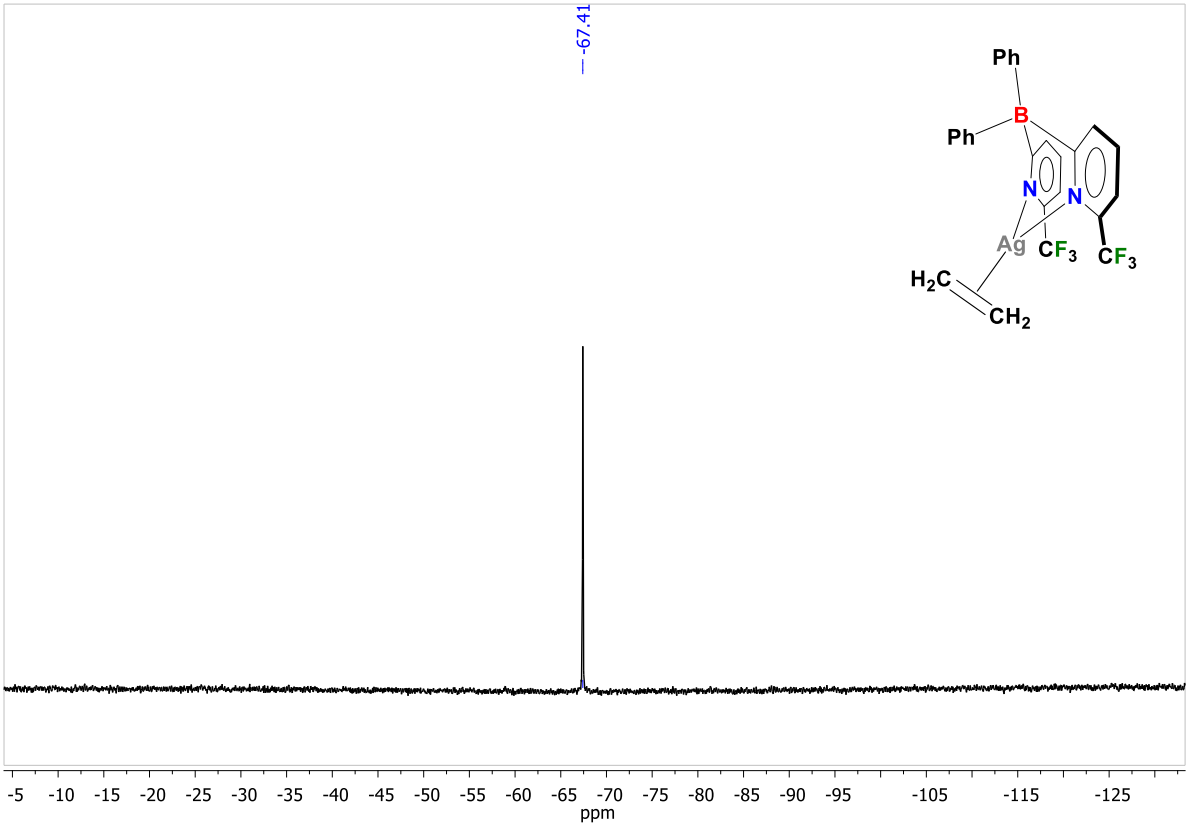

Figure S14. ^{19}F NMR spectrum of $[Ph_2B(6\text{-}(CF_3)Py)_2]Ag(C_2H_4)$ (**9**) in $CDCl_3$

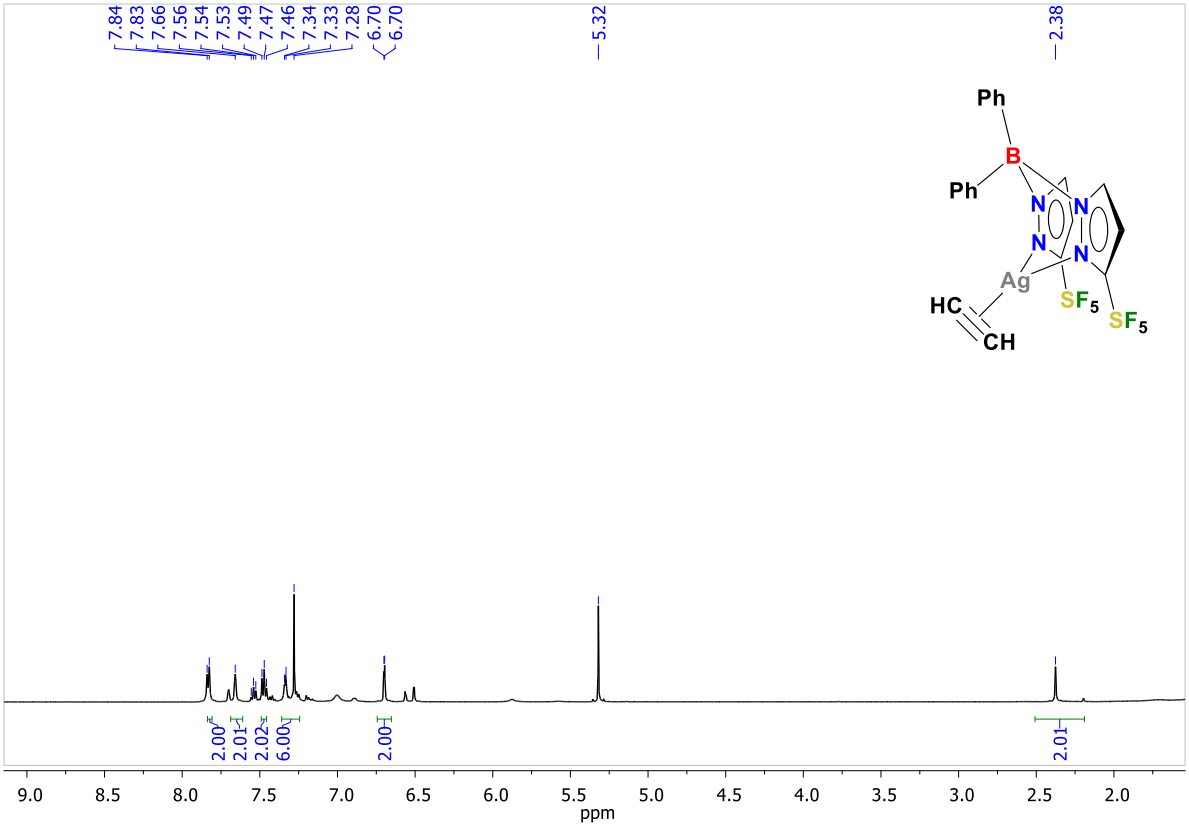

Figure S15. ^{1}H NMR spectrum of $[Ph_2B(3\text{-}(SF_5)Pz)_2]Ag(C_2H_2)$ (**10**) in CD_2Cl_2

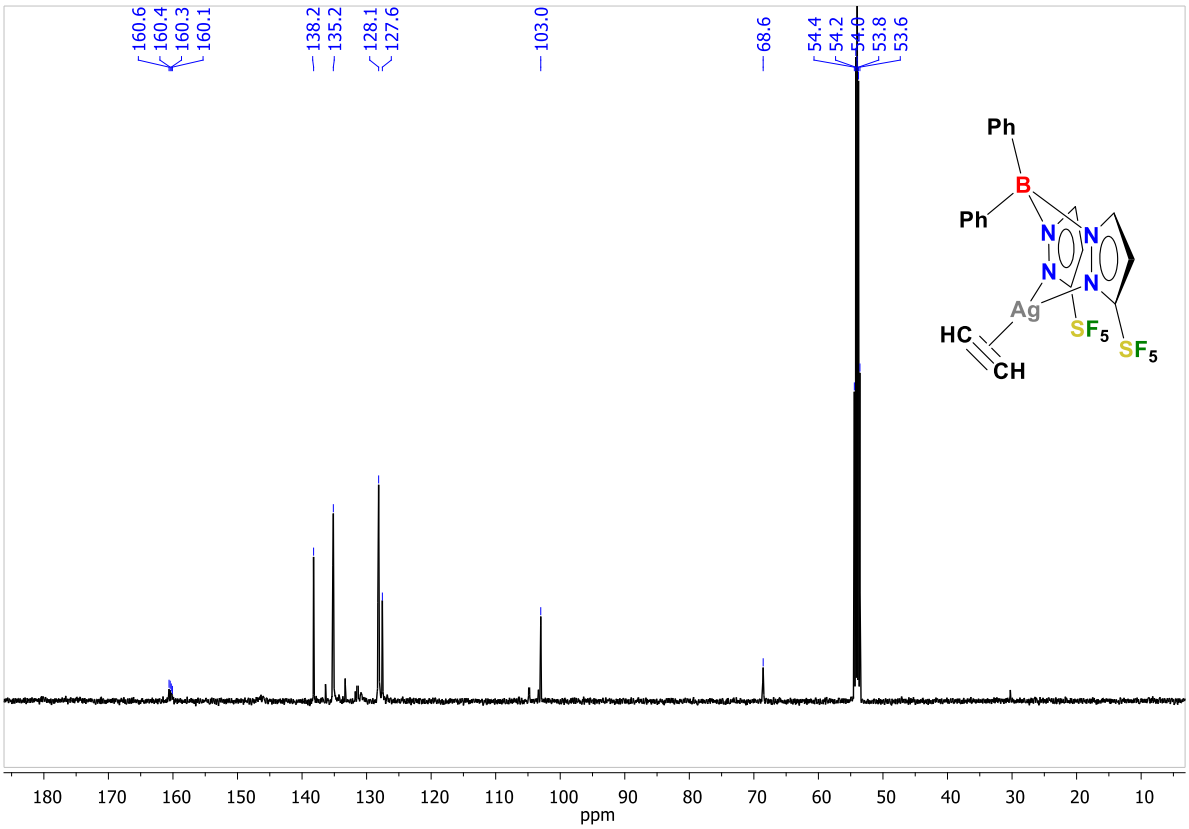

Figure S16. $^{13}C\{^{1}H\}$ NMR spectrum of $[Ph_2B(3\text{-}(SF_5)Pz)_2]Ag(C_2H_2)$ (**10**) in CD_2Cl_2

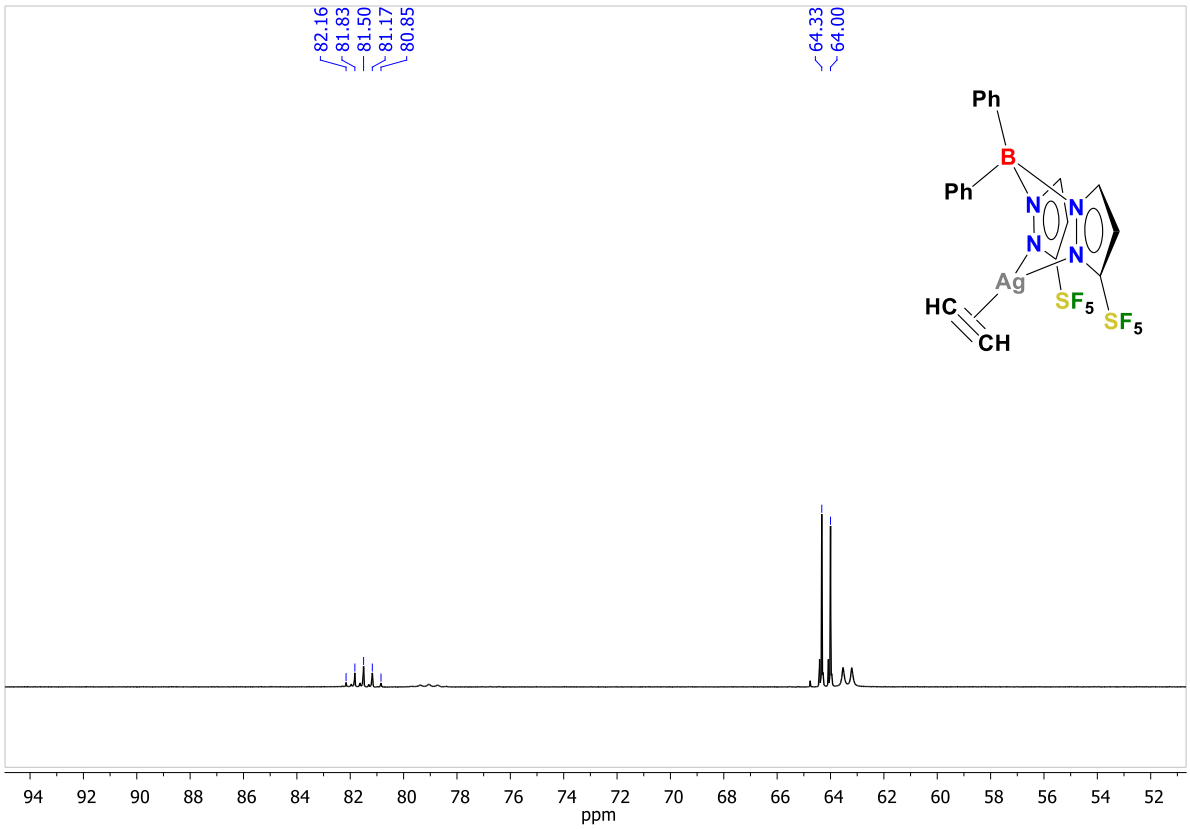

Figure S17. ^{19}F NMR spectrum of $[Ph_2B(3\text{-}(SF_5)Pz)_2]Ag(C_2H_2)$ (**10**) in $CDCl_3$

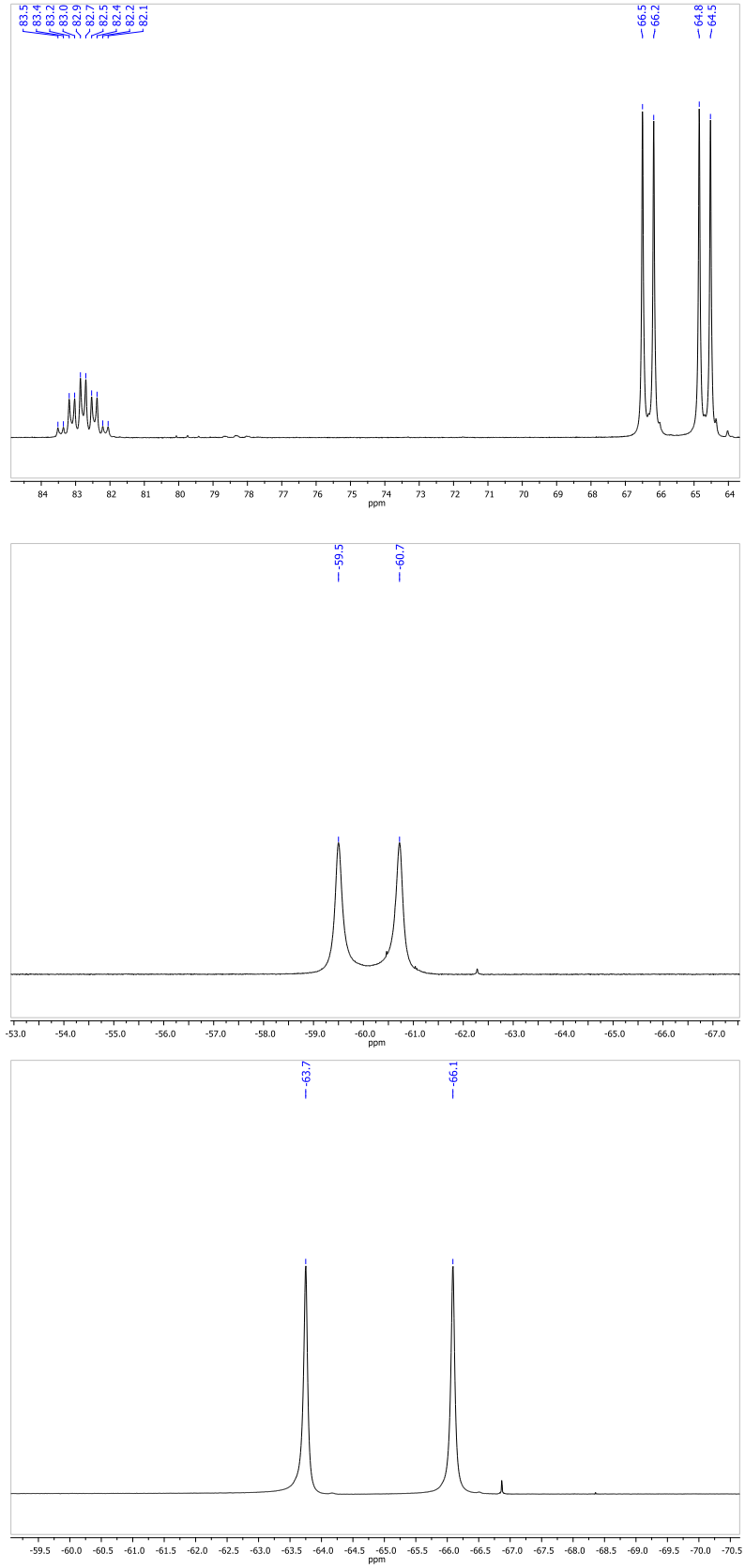

Figure S18. Comparison of ^{19}F NMR spectra of $[Ph_2B(3\text{-}(SF_5)Py)_2]Tl$ (**5**, top),[1] $[Ph_2B(3\text{-}(CF_3)Pz)_2]Tl$ (**4**, middle),[1] and $[Ph_2B(6\text{-}(CF_3)Py)_2]Tl$ (**6,** bottom) in $CDCl_3$ solution. In complex **5**, couplings between non-equivalent F_{axial} and $F_{equatorial}$ and Tl gave rise to a pentet of doublets and a doublet of doublets.

X-ray Data Collection and Structure Determinations

Table S2. Crystal data and structure refinement for of $[Ph_2B(3\text{-}(CF_3)Pz)_2]Tl$ (**4**)

Identification code	HRD6a
Empirical formula	$C_{20}H_{14}BF_6N_4Tl$
Formula weight	639.53
Temperature/K	100.0
Crystal system	orthorhombic
Space group	Pnma
a/Å	11.9158(3)
b/Å	10.0878(2)
c/Å	16.8524(4)
α/°	90
β/°	90
γ/°	90
Volume/Å^3	2025.73(8)
Z	4
ρ_{calc}g/cm^3	2.097
μ/mm^{-1}	8.043
F(000)	1208.0
Crystal size/mm^3	0.21 × 0.13 × 0.12
Radiation	Mo Kα (λ = 0.71073)
2Θ range for data collection/°	5.818 to 58.258
Index ranges	$-16 \leq h \leq 16$, $-13 \leq k \leq 13$, $-23 \leq l \leq 23$
Reflections collected	29831
Independent reflections	2876 [R_{int} = 0.0234, R_{sigma} = 0.0112]
Data/restraints/parameters	2876/0/160
Goodness-of-fit on F^2	1.052
Final R indexes [I>=2σ (I)]	R_1 = 0.0191, wR_2 = 0.0385
Final R indexes [all data]	R_1 = 0.0221, wR_2 = 0.0403
Largest diff. peak/hole / e Å^{-3}	1.78/-1.56

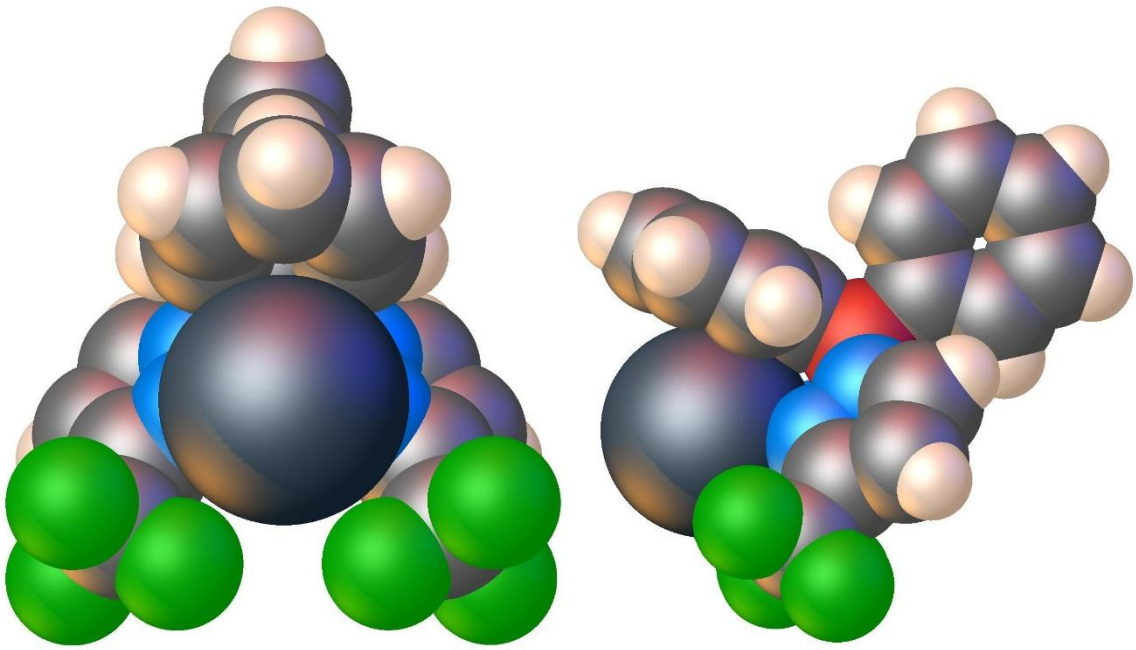

Figure S19. Two views of the space-filling model of the molecular structure of $[Ph_2B(3\text{-}(CF_3)Pz)_2]Tl$

Table S3. Crystal data and sucture refinement for of $[Ph_2B(3\text{-}(SF_5)Pz)_2]Tl$ (**5**)

Identification code	HRD29
Empirical formula	$C_{18}H_{14}BF_{10}N_4S_2Tl$
Formula weight	755.63
Temperature/K	100.0
Crystal system	triclinic
Space group	P-1
a/Å	11.4445(4)
b/Å	14.4529(5)
c/Å	15.6856(6)
α/°	88.495(2)
β/°	74.164(2)
γ/°	67.788(2)
Volume/Å^3	2302.17(15)
Z	4
ρ_{calc}g/cm^3	2.180
μ/mm^{-1}	7.294
F(000)	1432.0
Crystal size/mm^3	0.42 × 0.33 × 0.169
Radiation	Mo Kα (λ = 0.71073)
2Θ range for data collection/°	5.754 to 61.014
Index ranges	$-16 \leq h \leq 16$, $-20 \leq k \leq 20$, $-22 \leq l \leq 22$
Reflections collected	38141
Independent reflections	13883 [R_{int} = 0.0207, R_{sigma} = 0.0223]
Data/restraints/parameters	13883/0/650
Goodness-of-fit on F^2	1.058
Final R indexes [I>=2σ (I)]	R_1 = 0.0248, wR_2 = 0.0582
Final R indexes [all data]	R_1 = 0.0289, wR_2 = 0.0597
Largest diff. peak/hole / e Å^{-3}	2.50/-2.23

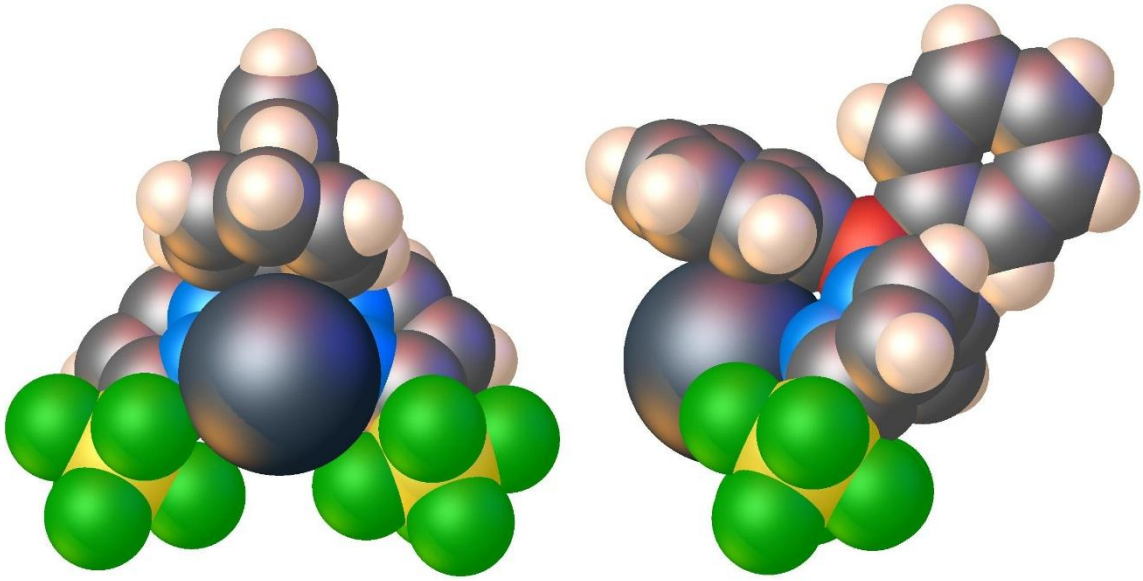

Figure S20. Two views of the space-filling model of the molecular structure of $[Ph_2B(3\text{-}(SF_5)Pz)_2]Tl$

Table S4. Crystal data and structure refinement for of $[Ph_2B(6\text{-}(CF_3)Py)_2]Tl$ (**6**)

Identification code	dia45
Empirical formula	$C_{24}H_{16}BF_6N_2Tl$
Formula weight	661.57
Temperature/K	99.99
Crystal system	triclinic
Space group	P-1
a/Å	10.178(2)
b/Å	10.282(2)
c/Å	10.926(2)
α/°	87.878(3)
β/°	77.995(3)
γ/°	82.193(3)
Volume/Å^3	1108.0(4)
Z	2
ρ_{calc}g/cm^3	1.983
μ/mm^{-1}	7.354
F(000)	628.0
Crystal size/mm^3	0.213 × 0.121 × 0.08
Radiation	Mo Kα (λ = 0.71073)
2Θ range for data collection/°	3.812 to 61.044
Index ranges	$-14 \leq h \leq 14$, $-14 \leq k \leq 14$, $-15 \leq l \leq 15$
Reflections collected	12727
Independent reflections	6369 [R_{int} = 0.0217, R_{sigma} = 0.0352]
Data/restraints/parameters	6369/0/307
Goodness-of-fit on F^2	1.039
Final R indexes [I>=2σ (I)]	R_1 = 0.0253, wR_2 = 0.0569
Final R indexes [all data]	R_1 = 0.0299, wR_2 = 0.0587
Largest diff. peak/hole / e Å^{-3}	1.49/-0.61

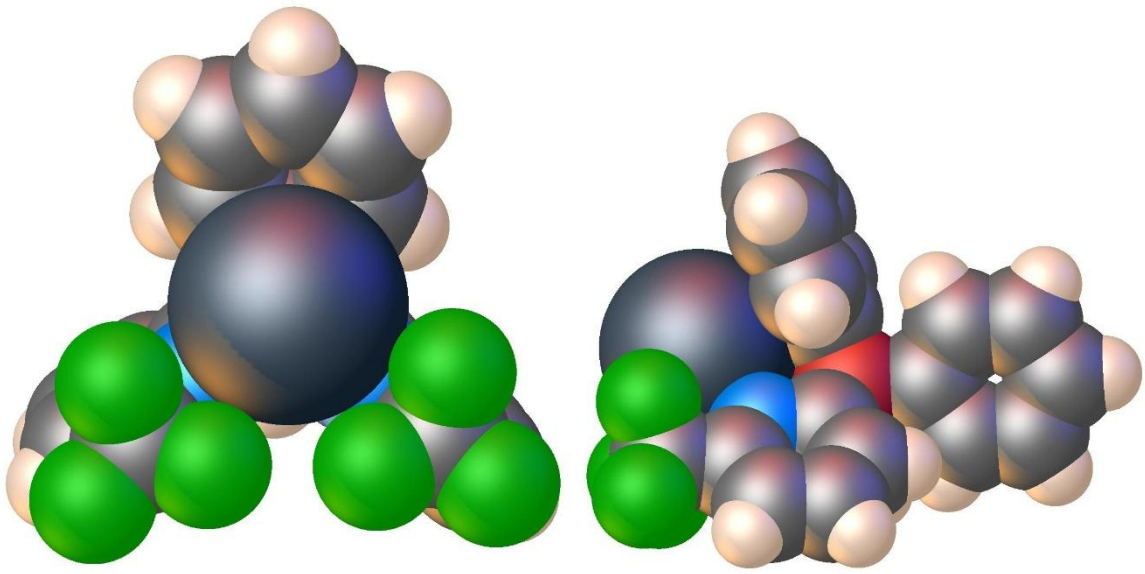

Figure S21. Two views of the space-filling model of the molecular structure of $[Ph_2B(6\text{-}(CF_3)Py)_2]Tl$

Table S5. Crystal data and structure refinement for of $[Ph_2B(3\text{-}(CF_3)Pz)_2]Ag(C_2H_4)$ (**7**)

Identification code	rad825
Empirical formula	$C_{22}H_{18}AgBF_6N_4$
Formula weight	571.08
Temperature/K	100.0
Crystal system	triclinic
Space group	P-1
a/Å	12.2646(6)
b/Å	17.0628(8)
c/Å	17.8516(8)
α/°	65.2530(10)
β/°	87.773(2)
γ/°	86.014(2)
Volume/Å^3	3384.3(3)
Z	6
ρ_{calc}g/cm^3	1.681
μ/mm^{-1}	0.961
F(000)	1704.0
Crystal size/mm^3	0.35 × 0.34 × 0.05
Radiation	MoKα (λ = 0.71073)
2Θ range for data collection/°	5.266 to 65.528
Index ranges	$-18 \leq h \leq 18$, $-25 \leq k \leq 25$, $-27 \leq l \leq 27$
Reflections collected	218516
Independent reflections	24981 [R_{int} = 0.0611, R_{sigma} = 0.0416]
Data/restraints/parameters	24981/15/948
Goodness-of-fit on F^2	1.031
Final R indexes [I>=2σ (I)]	R_1 = 0.0448, wR_2 = 0.0761
Final R indexes [all data]	R_1 = 0.0709, wR_2 = 0.0858
Largest diff. peak/hole / e Å^{-3}	1.20/-1.08

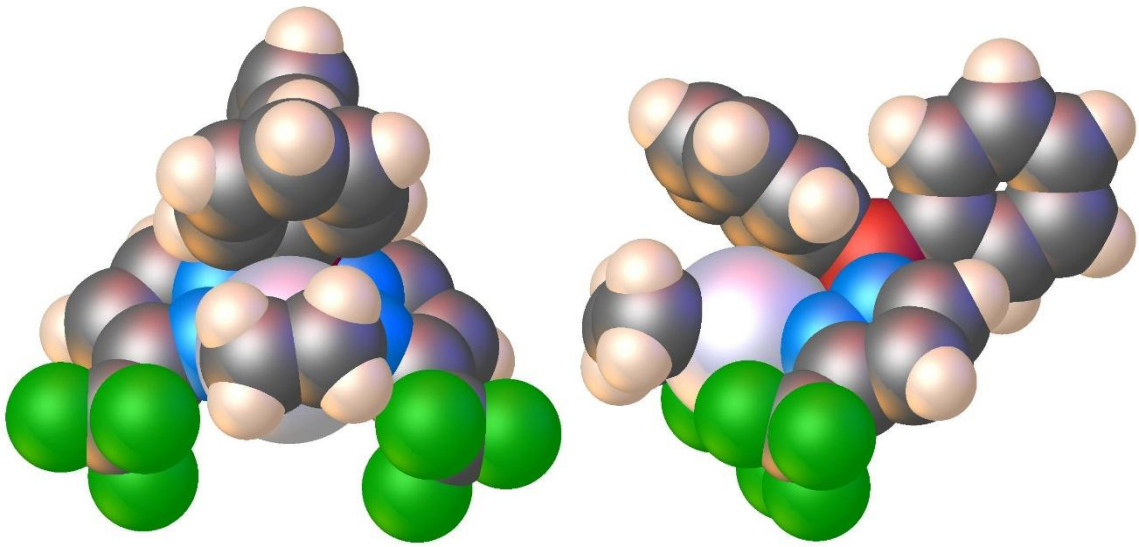

Figure S22. Two views of the space-filling model of the molecular structure of $[Ph_2B(3\text{-}(CF_3)Pz)_2]Ag(C_2H_4)$

Table S6. Crystal data and structure refinement for of $[Ph_2B(3\text{-}(SF_5)Pz)_2]Ag(C_2H_4)$ (**8**)

Identification code	dia17
Empirical formula	$C_{20.5}H_{19}AgBClF_{10}N_4S_2$
Formula weight	729.65
Temperature/K	99.98
Crystal system	monoclinic
Space group	$P2_1/c$
a/Å	20.1677(12)
b/Å	19.4767(12)
c/Å	13.7339(8)
α/°	90
β/°	96.5740(10)
γ/°	90
Volume/Å^3	5359.2(6)
Z	8
ρ_{calc}g/cm^3	1.809
μ/mm^{-1}	1.097
F(000)	2888.0
Crystal size/mm^3	0.38 × 0.32 × 0.24
Radiation	MoKα (λ = 0.71073)
2Θ range for data collection/°	2.916 to 62.106
Index ranges	$-29 \leq h \leq 28$, $-27 \leq k \leq 27$, $-19 \leq l \leq 18$
Reflections collected	61774
Independent reflections	16075 [R_{int} = 0.0171, R_{sigma} = 0.0164]
Data/restraints/parameters	16075/76/749
Goodness-of-fit on F^2	1.031
Final R indexes [I>=2σ (I)]	R_1 = 0.0258, wR_2 = 0.0635
Final R indexes [all data]	R_1 = 0.0291, wR_2 = 0.0655
Largest diff. peak/hole / e Å^{-3}	1.74/-1.29

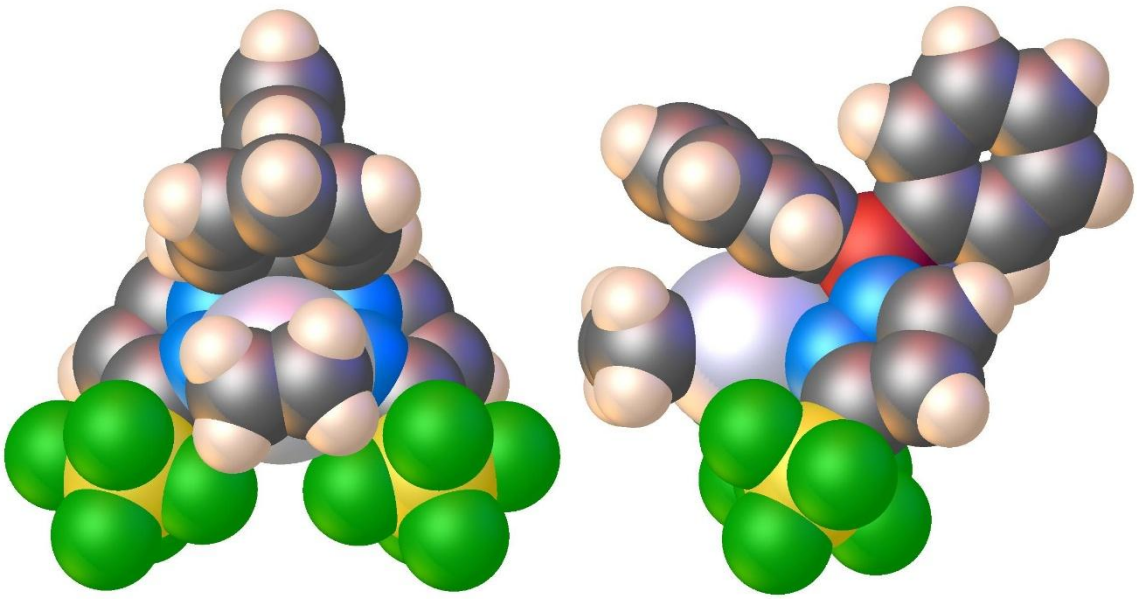

Figure S23. Two views of the space-filling model of the molecular structure of $[Ph_2B(3\text{-}(SF_5)Pz)_2]Ag(C_2H_4)$

Table S7. Crystal data and structure refinement for of $[Ph_2B(6\text{-}(CF_3)Py)_2]Ag(C_2H_4)$ (**9**)

Identification code	dia56
Empirical formula	$C_{27}H_{22}AgBCl_2F_6N_2$
Formula weight	678.04
Temperature/K	99.98
Crystal system	monoclinic
Space group	$P2_1/c$
a/Å	15.9889(12)
b/Å	16.2352(13)
c/Å	10.0306(8)
α/°	90
β/°	91.3820(10)
γ/°	90
Volume/Å^3	2603.0(4)
Z	4
ρ_{calc}g/cm^3	1.730
μ/mm^{-1}	1.044
F(000)	1352.0
Crystal size/mm^3	0.49 × 0.3 × 0.157
Radiation	Mo Kα (λ = 0.71073)
2Θ range for data collection/°	3.576 to 62
Index ranges	$-23 \leq h \leq 22$, $-23 \leq k \leq 22$, $-14 \leq l \leq 13$
Reflections collected	29779
Independent reflections	7804 [R_{int} = 0.0153, R_{sigma} = 0.0135]
Data/restraints/parameters	7804/0/368
Goodness-of-fit on F^2	1.032
Final R indexes [I>=2σ (I)]	R_1 = 0.0202, wR_2 = 0.0489
Final R indexes [all data]	R_1 = 0.0220, wR_2 = 0.0497
Largest diff. peak/hole / e Å^{-3}	1.04/-1.05

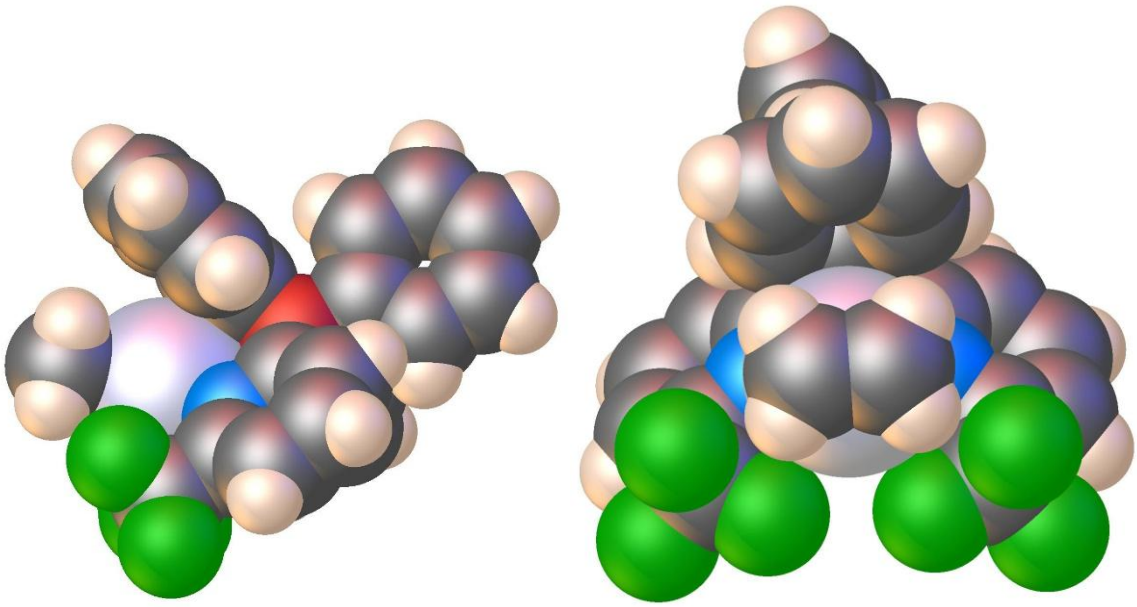

Figure S24. Two views of the space-filling model of the molecular structure of $[Ph_2B(6\text{-}(CF_3)Py)_2]Ag(C_2H_4)$

Silver mediated C-H functionalization of alkanes

General procedures: To a 10 mL Schlenk flask containing silver catalyst (5 mol %), 3 mL of alkane substrate was added under inert atmosphere, followed by addition of ethyl diazoacetate (0.3 mmol, 1 equiv.) in one portion. The reaction mixture was stirred at room temperature for 8 h. Volatiles were removed under vacuum, and the reaction yield was determined by ^{1}H NMR spectroscopy using 1,3,5-tris(trifluoromethyl)benzene as an internal standard.

Table S8. Products from the functionalization of C–H bonds via carbene insertion into hydrocarbons using ethyl diazoacetate (EDA) as the carbene source

Substrate	Primary C-H products	Secondary C-H products	Tertiary C-H products
	-	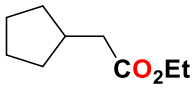	-
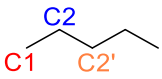	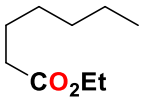	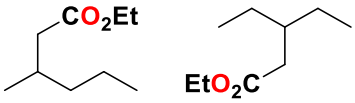	-
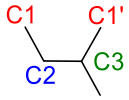	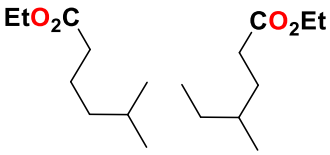	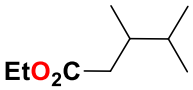	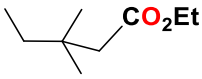
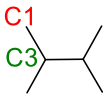	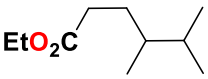	-	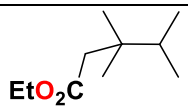

Table S9. Product yields for C–H functionalization of hydrocarbons via carbene insertion from ethyl diazoacetate catalyzed by bis(pyrazolyl/pyridyl)borate silver complexes [$Ph_2B(3\text{-}(CF_3)Pz)_2]Ag(C_2H_4)$ (**7**), [$Ph_2B(3\text{-}(SF_5)Pz)_2]Ag(C_2H_4)$ (**8**), and [$Ph_2B(6\text{-}(CF_3)Py)_2]Ag(C_2H_4)$ (**9**)

catalyst		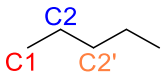	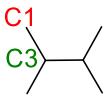	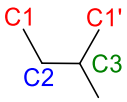
7[c]	**90**	**24:53:16**	**42:54**	**37**[b]**:24:26**
8[c]	**89**	**28:44:17**	**47:43**	**35**[b]**:28:24**
9[d]	**61**	**19:30:7**	**24:14**	**30**[b]**:14:12**

[a]Product yields (%) of each site

[b]The total yield (%) at primary sites

[c]In case of catalyst **7** and **8**, the EDA consumptions were 100%, the remaining carbene fragments accounted for the formation of diethyl fumarate and diethyl maleate as byproducts

[d]In case of catalyst **9**, the product mixtures contained unreactive EDA, diethyl fumarate and diethyl maleate

References

1. A. Noonikara-Poyil, A. Munoz-Castro, A. Boretskyi, P. K. Mykhailiuk and H. V. R. Dias, *Chem. Sci.*, 2021, **12**, 14618–14623.
2. O. Renn, L. M. Venanzi, A. Marteletti and V. Gramlich, *Helv. Chim. Acta*, 1995, **78**, 993–1000.
3. H. V. R. Dias and J. Thankamani, *Acta Crystallogr., Sect. C Cryst. Struct. Commun.*, 2013, **69**, 959–962.
4. M. Vanga, V. Q. H. Phan, J. Wu, A. Muñoz-Castro and H. V. R. Dias, *Inorg. Chem.*, 2023, **62**, 18563–18572.
5. E. R. Sirianni, G. P. A. Yap and K. H. Theopold, *Inorg. Chem.*, 2014, **53**, 9424–9430.
6. R. Han, P. Ghosh, P. J. Desrosiers, S. Trofimenko and G. Parkin, *J. Chem. Soc., Dalton Trans.*, 1997, 3713–3718.
7. H. V. R. Dias, X. Wang and H. V. K. Diyabalanage, *Inorg. Chem.*, 2005, **44**, 7322–7324.
8. H. V. Rasika Dias and T. K. H. H. Goh, *Polyhedron*, 2004, **23**, 273–282.
9. R. Gava, A. Olmos, B. Noverges, T. Varea, E. Álvarez, T. R. Belderrain, A. Caballero, G. Asensio and P. J. Pérez, *ACS Catal.*, 2015, **5**, 3726–3730.
10. L. Falivene, Z. Cao, A. Petta, L. Serra, A. Poater, R. Oliva, V. Scarano and L. Cavallo, *Nature Chem.*, 2019, **11**, 872–879.